J. Fluid Mech. (2003), *vol.* 491, *pp.* 101–129.
DOI: 10.1017/S0022112003005263 Printed in the United Kingdom

Receptivity of a high-speed boundary layer to acoustic disturbances

By ALEXANDER V. FEDOROV

Department of Aeromechanics and Flight Engineering, Moscow Institute of Physics and Technology, Zhukovski, 140180, Russia

(Received 19 August 2002 and in revised form 18 April 2003)

Receptivity of a high-speed boundary layer on a flat plate to acoustic disturbances is investigated using a combined numerical and asymptotic approach. The leading-edge receptivity problem is discussed with emphasis on physical mechanisms associated with scattering and diffraction of acoustic waves. Analytical solutions provide insight into the interplay of these mechanisms as a function of the angle of incidence of external acoustic waves. The theoretical predictions are in good agreement with the wind-tunnel experimental data of Maslov *et al.* obtained at free-stream Mach number 6. The leading-edge receptivity model is incorporated into the multiple-modes method to account for the inter-modal exchange downstream from the leading edge. This combined modelling resembles basic features of the direct numerical simulation of Ma & Zhong. A comparative analysis of the leading-edge receptivity and the inter-modal exchange associated with non-parallel effects is presented. The theory allows fast evaluation of the receptivity coefficients and clarifies the physics of the receptivity process. The theoretical results may guide further direct numerical simulations and experimental studies of boundary layer receptivity at supersonic and hypersonic speeds.

1. Introduction

The receptivity problem is associated with excitation of the boundary-layer modes by free-stream disturbances (acoustic, vortical and thermal perturbations) and by wall-induced disturbances (vibrations, periodic suction/blowing and surface heating), see Morkovin (1969), Reshotko (1976). Solutions of this problem provide initial conditions for the initial boundary-value problem describing the downstream evolution of unstable disturbances. Incorporating results of receptivity studies into the transition prediction methodology is desirable in order to couple the transition locus with characteristics of free-stream disturbances and avoid the empiricism of the e^N-method (Malik, Zang & Bushnell 1990).

For subsonic boundary layers, when the phase speeds of free-stream disturbances and Tollmien–Schlichting (TS) waves are significantly different, the main objective of receptivity studies is to identify a scale-conversion mechanism tuning the time and/or length scales of external disturbances. Theoretical analyses of Goldstein (1983, 1985), Ruban (1984), Zhigulev & Fedorov (1987) and the later studies of Choudhari & Streett (1990) and Choudhari (1994, 1996) showed that acoustic waves may effectively generate TS waves if the forcing length scale is of the order of the TS wavelength. This can be achieved in non-parallel flows near the leading edge, in the vicinity of a surface imperfection, or over a wavy wall or hump. Choudhari & Streett (1990)

suggested a different mechanism associated with the bilinear interaction between a pair of free-stream disturbances. Wu (1999) elaborated this mechanism by considering suitable convecting gusts, which interact with sound waves to produce a forcing that has the same time and length scales as those of TS waves in the vicinity of the neutral point. In this case, the scale conversion is achieved without resorting to a local non-homogeneity of the mean flow.

The stability experiments of Kendall (1975) showed that the evolution of disturbances in the supersonic boundary layer on a flat plate at Mach numbers 3, 4.5 and 5.6 is essentially different from the case of subsonic flows. Kendall reported that "fluctuations of all frequencies were observed to grow monotonically larger in the region of a boundary layer extending from the flat plate leading edge to the predicted location of instability; i.e. in a region where no growth was expected". Similar observations were reported by Stetson *et al.* (1991) for a planar boundary layer at Mach 8 and by Graziosi & Brown (2002) for the boundary layer on a flat plate at Mach 3. Mack (1975) developed a forcing theory, which was successfully applied to the Mach 4.5 data of Kendall (1975). However, Mack noted that "the major difficulty in the use of the forcing theory is that forced disturbances are distinct from free disturbances, and the process by which the former becomes the latter is unknown".

These findings motivated further theoretical studies of the disturbance field in the leading-edge region. Fedorov & Khokhlov (1991, 1993, 2001) showed that the disturbance spectrum reveals new features in boundary layers at supersonic and, especially, hypersonic speeds when the second mode becomes the dominant instability. These features are illustrated in figure 1 where the phase speeds of two-dimensional disturbances are shown as a function of the Reynolds number $R = \sqrt{U_\infty^* x^* / \nu_\infty^*}$ (where U_∞^* is the free-stream velocity, x^* the distance from the leading edge and ν^* the kinematic viscosity) for the boundary layer on a flat plate at the free-stream Mach number $M = 4.5$, the wall temperature ratio $T_w / T_{ad} = 1$ and the frequency parameter $F = 5 \times 10^{-5}$. In the leading-edge region 1, the boundary-layer modes are synchronized with acoustic waves. Namely, the wavenumber of one mode (Mode S in figure 1) tends to the wavenumber of slow acoustic wave with the phase speed $c = 1 - 1/M$, whereas the wavenumber of another mode (Mode F in figure 1) tends to that of fast acoustic wave with $c = 1 + 1/M$. This leads to significant changes of the disturbance field structure in the leading-edge vicinity. Early studies by Gaponov (1983, 1985) led to similar conclusions. In Region 2, Mode F is synchronized with the external entropy/vorticity waves of phase speed $c = 1$. The disturbance dynamics associated with this synchronization was analysed by Fedorov & Tumin (2001). Near the lower neutral branch of Mode S (Region 3), Mode F is synchronized with Mode S that leads to discrete spectrum branching. Fedorov & Khokhlov (2002) showed that in this region the boundary layer is extremely receptive to wall-induced disturbances such as vibrations and periodic suction–blowing.

Because the time and length scales of synchronized disturbances are close to each other, a strong interaction occurs between them without resorting to the scale-convergence mechanism. Moreover, the difference between the phase speeds of the boundary-layer modes and those of acoustic waves is relatively small in a wide region (from the leading edge to the upper neutral branch). This difference decreases with the Mach number, which may enhance the distributed inter-modal exchange.

Using asymptotic methods Fedorov & Khokhlov (1991, 1993) developed a theoretical model that predicted the leading-edge receptivity coefficients in a compact analytical form. This model provides insight into the physics of local receptivity

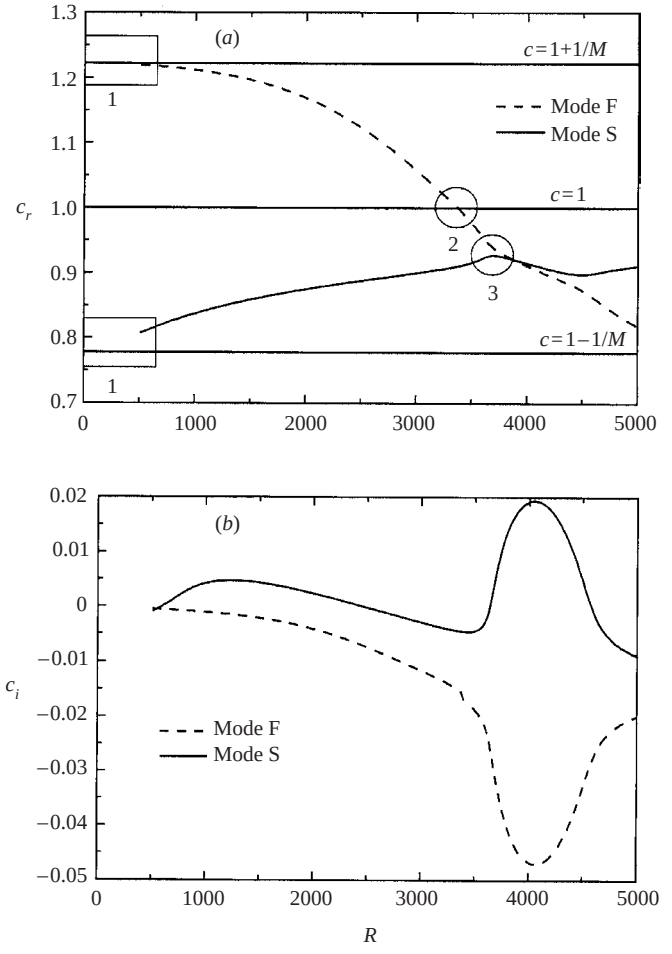

FIGURE 1. Phase speed of two-dimensional disturbances as a function of Reynolds number $R = \sqrt{U_\infty^* x^* / \nu_\infty^*}$; $M = 4.5$, $T_w/T_{ad} = 1$, $F = 5 \times 10^{-5}$.

associated with diffraction and scattering of acoustic waves near a sharp leading edge. Further downstream, the mean-flow non-parallel effect leads to distributed receptivity due to the inter-modal exchange on a relatively large length scale. This mechanism couples amplitudes of different modes via longitudinal variations of the mean flow. The inter-modal exchange can be modelled using the multiple-modes method discussed by Zhigulev & Tumin (1987) and Fedorov & Khokhlov (2001). A combination of the two methods allows modelling of disturbance dynamics in both the leading-edge and downstream regions. This also helps a comparison of the inter-modal exchange with the leading-edge receptivity.

Recently Maslov *et al.* (2001) performed wind-tunnel experiments on receptivity of the boundary layer to two-dimensional and three-dimensional acoustic disturbances interacting with a sharp leading edge of a flat plate at the free-stream Mach number $M_\infty = 5.92$. These data provide an opportunity to verify the theoretical model of Fedorov & Khokhlov (1991, 1993). The direct numerical simulation (DNS) of Ma & Zhong (2001) gives another opportunity to compare theoretical predictions with the numerical experiment on receptivity to two-dimensional acoustic waves at $M_\infty = 4.5$.

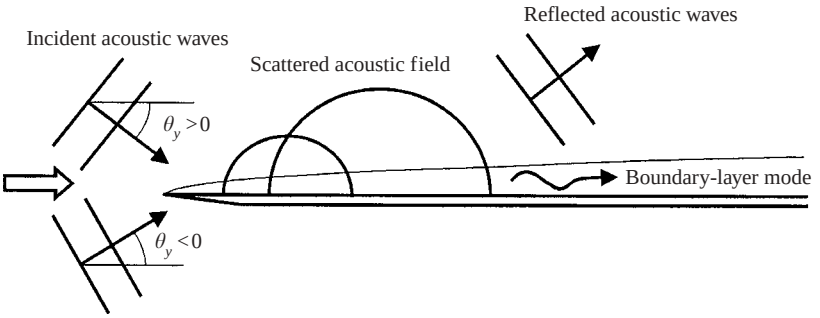

FIGURE 2. Physical picture of the disturbance field.

This has motivated us to revise the theory of Fedorov & Khokhlov (1991, 1993), incorporate its results into the multiple-modes method accounting for an inter-modal exchange and verify the theoretical predictions by comparison with the experimental data and DNS.

In § 2, we briefly outline the theoretical model of leading-edge receptivity to acoustic disturbances interacting with a sharp flat plate at supersonic speeds. The discussion is focused on physical aspects of the problem and comparisons with the experiment of Maslov *et al.* (2001). Interested readers are referred to Fedorov & Khokhlov (1991, 1993) for mathematical details. In § 3, we consider an exchange between the boundary-layer modes due to non-parallel effects and compare the results with the DNS of Ma & Zhong (2001). We also discuss a relationship between the leading-edge receptivity and the inter-modal exchange. In § 4, we conclude the paper with a summary discussion.

2. Leading-edge receptivity

2.1. *Asymptotic structure of the disturbance field*

Consider the supersonic flow over a semi-infinite flat plate radiated by acoustic waves of angular frequency ω^* as schematically shown in figure 2. The flow density, temperature and velocity components (u, v, w) are referenced to their free-stream values ρ_∞^*, T_∞^* and U_∞^*, where an asterisk denotes a dimensional quantity. The quantities $\omega^{*^{-1}}$, $\Lambda^* = U_\infty^*/\omega^*$ and $\rho_\infty^* U_\infty^{*2}$ are used as reference time, length and pressure, respectively. Since the disturbance phase speed is $\sim U_\infty^*$, the length scale Λ^* is of the order of the disturbance wavelength. The non-dimensional frequency parameter $F = \nu_\infty^* \omega^*/U_\infty^{*2}$ is assumed to be small ($F \sim 10^{-5}$–10^{-4} for unstable disturbances). It is also assumed that the disturbance amplitude is small enough for the linear theory to be applicable.

In uniform flow (outside the boundary layer), pressure fluctuations are governed by the linear acoustic equation, which has the elementary wave solution with wave-vector components (α, γ, β)

$$p = \exp(\mathrm{i}\alpha x + \mathrm{i}\gamma y + \mathrm{i}\beta z - \mathrm{i}t), \tag{2.2}$$

$$\gamma = \sqrt{(M^2-1)(\alpha-\alpha_1)(\alpha-\alpha_2)}, \quad \alpha_{1,2} = \frac{M^2 \pm \sqrt{M^2 + \beta^2(M^2-1)}}{M^2-1}, \tag{2.3}$$

where $M > 1$ is free-stream Mach number. For β real and fixed, the branch points $\alpha_{1,2}$ of the function $\gamma(\alpha)$ correspond to slow and fast acoustic waves with the wave

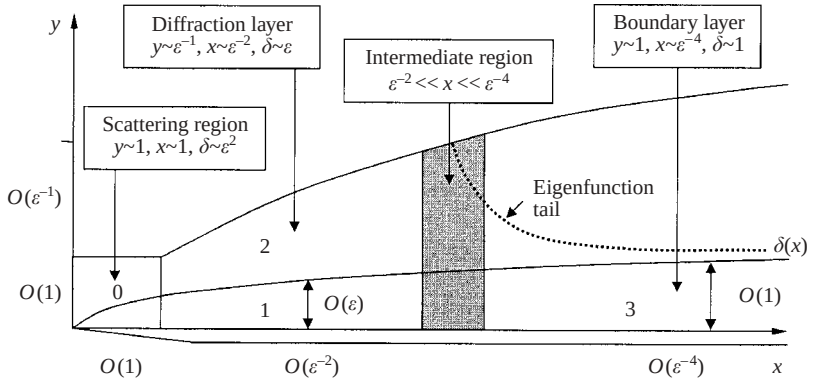

FIGURE 3. Asymptotic structure of the disturbance field.

front being perpendicular to the plate surface. In this case, the angle of incidence $\theta_y = \tan^{-1}(\gamma/\alpha) = 0$, the sweep angle $\theta_z = \tan^{-1}(\beta/\alpha)$, and the vertical wavenumber $\gamma(\alpha_{1,2}) = 0$. The wavenumbers $\alpha_{1,2}$ and the correspondent phase speeds $c_{1,2} = 1/\alpha_{1,2}$ can be written in terms of θ_z as

$$\alpha_{1,2} = \frac{M\cos\theta_z}{M\cos\theta_z \mp 1}, \quad c_{1,2} = 1 \mp \frac{1}{M\cos\theta_z}. \tag{2.4}$$

The wavenumber ranges $\alpha > \alpha_1$ and $\alpha < \alpha_2$ are related to slow and fast acoustic waves with the angles of incidence $\theta_y \neq 0$. For $\theta_y > 0$ (the waves are incident on the plate from above) the branch of $\gamma(\alpha)$ is chosen as $\arg(\gamma(\alpha > \alpha_1)) = 0$ and for $\theta_y < 0$ (the waves are incident on the plate from below) $\arg(\gamma(\alpha > \alpha_1)) = -\pi$. The wavenumbers are expressed in terms of the wave-front angles as

$$\alpha = \frac{M\cos\theta_y\cos\theta_z}{M\cos\theta_y\cos\theta_z \pm 1}, \tag{2.5}$$

where plus (minus) corresponds to fast (slow) acoustic waves.

The presence of a thin plate leads to reflection of the incident wave, diffraction of the disturbance due to the boundary layer growth, and scattering of the incident wave by the leading edge. For $\theta_y = 0$ diffraction is the dominant mechanism since the leading-edge scattering is negligible. For $\theta_y < 0$ both scattering and diffraction affect the disturbance field. For $\theta_y > 0$ incident and reflected acoustic waves are involved in the receptivity process.

First, we consider acoustic waves with the wavenumbers $\alpha = \alpha_{1,2}$ when $\theta_y = 0$. In the inviscid limit, when the boundary layer is negligibly thin, the pressure disturbance is given by (2.2) with $\gamma = 0$. For finite but small viscosity, the boundary layer on the plate surface disturbs the acoustic field. Fedorov & Khokhlov (1991, 1993) showed that an asymptotic structure of this disturbance is governed by the small parameter $\varepsilon = \Delta^{1/2}F^{1/4}$, where Δ is related to the boundary-layer displacement thickness as $\delta^* = \Delta\sqrt{\nu_\infty^* x^*/U_\infty^*}$. The coefficient Δ is a function of M and the wall temperature T_w. It is included in the asymptotic scaling in order to account for the strong dependence of the boundary-layer characteristics on these parameters. The disturbance-field scaling is given by the relations

$$x = (x_1, \varepsilon^{-2}x_2, \varepsilon^{-4}x_3), \quad y = (\varepsilon y_1, \varepsilon^{-1}y_2, y_3). \tag{2.6}$$

The asymptotic structure (2.6) is schematically shown in figure 3 (see also Fedorov &

Khokhlov 1991). It includes: the scattering region (0) with $(x, y) = O(1)$; the near-field boundary layer (1) with $(x_2, y_1) = O(1)$; the diffraction layer (2) with $(x_2, y_2) = O(1)$; the far-field boundary layer (3) with $(x_3, y_3) = O(1)$, which contains the lower and upper neutral branches of the unstable boundary-layer mode. The Stokes layer of the thickness $O(\varepsilon^2)$ is not depicted, since it has no influence on the disturbance field in the dominant approximation considered hereafter. The scaling (2.6) holds for slightly inclined acoustic waves with $\alpha - \alpha_{1,2} = O(\varepsilon^2)$ because additional distortions, which are due to the phase dependence on y, can be treated as slow variations of the disturbance amplitude. Moreover, (2.6) holds for a blunted plate only if the leading-edge radius r^* is small compared with the boundary-layer thickness in the diffraction layer: $r^*/\Lambda^* \ll \varepsilon$.

For disturbances of relatively high frequency, the wavelength may be of the order of the distance to the neutral branch, i.e. the parameter ε may be not very small. This case is exemplified by the stability experiments of Graziosi & Brown (2002) performed at relatively low unit Reynolds numbers. The first-order asymptotic theory discussed hereafter may fail to predict the receptivity coefficients in this range of parameters. However, the theoretical model may still be useful for capturing qualitative trends and providing insight into physical mechanisms of the receptivity process.

2.2. *Solution in the diffraction layer*

Under the assumptions of § 2.1 the disturbance wavelength is short relative to the diffraction-layer thickness and long relative to the boundary-layer thickness. In addition, the longitudinal length of the diffraction layer is much larger than the disturbance wavelength, while it is much smaller than the distance to the neutral branch. These properties allowed Fedorov & Khokhlov (1991, 1993) to obtain analytical solutions in the near-field region $x_2 = O(1)$. They considered slightly oblique acoustic waves with wavenumbers

$$\alpha = \alpha_{1,2} \pm \varepsilon^2 q^2, \quad q = O(1), \tag{2.7}$$

where $q > 0$ if the wave radiates the plate from above ($\theta_y > 0$), and $q < 0$ if the wave is incident on the plate from below ($\theta_y < 0$). In the dominant-order approximation, the pressure amplitude is constant across the boundary layer. Its dependence on the longitudinal coordinate x_2 is governed by the integral equation

$$p_1(x_2) - \lambda \int_0^{x_2} \sqrt{\frac{\xi}{x_2 - \xi}}\, p_1(\xi)\, \mathrm{d}\xi = \exp(\pm \mathrm{i} q^2 x_2) + \sqrt{\pm \mathrm{i}/\pi}\, q \int_0^{x_2} \frac{\exp(\pm \mathrm{i} q^2 \xi)}{\sqrt{x_2 - \xi}}\, \mathrm{d}\xi, \tag{2.8}$$

$$\lambda = -\frac{(\alpha_{1,2} - 1)^2 k}{\sqrt{2\pi \mathrm{i}[M^2(\alpha_{1,2} - 1) - \alpha_{1,2}]}}. \tag{2.9}$$

Here k is the integral parameter, which depends on the mean velocity U and temperature T as

$$k = \int_0^{\infty} \left[\frac{T\left(\alpha_{1,2}^2 + \beta^2\right)}{(\alpha_{1,2} U - 1)^2} - M^2 \right] \mathrm{d}\eta,$$

where $\eta = y_1/\sqrt{x_2}$ is the boundary-layer variable. For $q = 0$ ($\theta_y = 0$), the solution of (2.8) is expressed in the series form

$$p_1 = \sum_{n=0}^{\infty} a_n \pi^{n/2} (\lambda x_2)^n, \quad a_0 = 1, \quad a_n = \prod_{j=1}^{n} \frac{\Gamma(j + 1/2)}{\Gamma(j + 1)}, \tag{2.10}$$

where Γ is the gamma function. The downstream asymptotic expansion of (2.10) is

$$\left.\begin{aligned} p_1 &= E_0\left(\pi\lambda^2 x_2^2\right)^{1/8}\exp\left(\pi\lambda^2 x_2^2/2\right) - (\pi\lambda x_2)^{-1} + \ldots, \quad x_2 \to \infty, \\ E_0 &= (8\pi)^{1/4}A, \quad A = \lim_{n\to\infty}\left[n^{-1/8}a_n\sqrt{\Gamma(n+3/2)}\right] = 0.935\ldots. \end{aligned}\right\} \tag{2.11}$$

The first (exponential) term is a 'seed' for the boundary-layer modes. Since the parameter λ is essentially complex, this term has an oscillatory behaviour indicating that the incident acoustic wave evolves into another wave with the phase speed departing from its original value. Such a behaviour indicates that a portion of the acoustic disturbance is transferred to a boundary-layer mode.

The second term in (2.11) is associated with the acoustic disturbance decaying as x_2^{-1}, i.e. the boundary layer displaces the acoustic field and forms a quiescent layer over the plate surface. This result is consistent with the DNS depicted in figure 15 of Ma & Zhong (2001). At first glance, this contradicts the experimental data of Kendall (1975) indicating a monotonic growth of a wide range of frequencies from the leading edge to the upstream neutral branch. However, such a growth is observed for the maximum of mass-flow fluctuations in the boundary layer radiated by acoustic waves of non-zero angles θ_y. The behaviour of this maximum is quite different from that of the wall pressure disturbance induced by acoustic waves of $\theta_y = 0$.

Fedorov & Khokhlov (1993) showed that in the case of $q \neq 0$ the asymptotic solution also includes the exponential term with the constant E_0 being replaced by the function

$$E(q) = E_0\left[\varphi(r) + \sqrt{\pm\mathrm{i}/(\pi\lambda)}\,q\psi(r)\pi^{1/4}/A^2\right], \tag{2.12}$$

$$\varphi(r) = \sum_{n=0}^{\infty}\frac{\pi^{n/2}r^n}{a_n n!}, \quad \psi(r) = \sum_{n=0}^{\infty}\pi^{n/2}a_n r^n, \quad r = \pm\mathrm{i}q^2/(\pi\lambda). \tag{2.13}$$

The relation (2.12) determines the boundary-layer response to acoustic waves of small angles of incidence $\theta_y = O(\varepsilon)$.

2.3. *Boundary-layer modes*

Disturbances in the far-field boundary layer $(x_3, y_3) = O(1)$ (Region 3 in figure 3) were analysed by Fedorov & Khokhlov (1991, 1993) using the WKB method, which was applied by Gaster (1974) to incompressible boundary layers and extended to compressible flows by Nayfeh (1980) and Zhigulev & Tumin (1987). Since $\Lambda^* = U_\infty^*/\omega^*$ has been taken as a characteristic length scale, the Reynolds number is determined as $R_\Lambda = U_\infty^{*2}/(\omega^*\nu_\infty^*) = F^{-1}$. A three-dimensional disturbance is represented by the vector function

$$\boldsymbol{Z} = \left(u,\ \frac{\partial u}{\partial y},\ v,\ p,\ \vartheta,\ \frac{\partial\vartheta}{\partial y},\ w,\ \frac{\partial w}{\partial y}\right)^T, \tag{2.14}$$

$$\boldsymbol{Z} = \left[\boldsymbol{Z}_0(x_3, y) + \varepsilon^4\boldsymbol{Z}_1(x_3, y) + \ldots\right]\exp(\mathrm{i}\tilde{S}), \tag{2.15}$$

$$\tilde{S} = \varepsilon^{-4}\int_0^{x_3}\tilde{\alpha}(x_3)\,\mathrm{d}x_3 + \beta z - t,$$

where ϑ is the temperature fluctuation; $y = y_3$ according to (2.6). The amplitude function $\boldsymbol{Z}_0$ and the eigenvalue $\tilde{\alpha}$ are solutions of the standard boundary-value

problem for a locally parallel boundary layer

$$\frac{\partial \boldsymbol{Z}_0}{\partial y} = \boldsymbol{H}_0 \boldsymbol{Z}_0,$$
$$Z_{01} = Z_{03} = Z_{05} = Z_{07} = 0, \quad y = 0, \tag{2.16}$$
$$|\boldsymbol{Z}_0| \to 0, \quad y \to \infty.$$

Here $\boldsymbol{H}_0$ is 8×8 matrix, which depends on the mean-flow profiles $U(x_3, y)$ and $T(x_3, y)$, disturbance parameters $\tilde{\alpha}$, β and the Reynolds number R_Λ. Non-zero elements of $\boldsymbol{H}_0$ are given in the Appendix of Fedorov & Khokhlov (2002). At the next-order approximation, the problem is formulated as

$$\left(\frac{\partial}{\partial y} - \boldsymbol{H}_0\right) \boldsymbol{Z}_1 = -\mathrm{i}\frac{\partial \boldsymbol{H}_0}{\partial \tilde{\alpha}} \frac{\partial \boldsymbol{Z}_0}{\partial x_3} + \boldsymbol{H}_1 \boldsymbol{Z}_0,$$
$$Z_{11} = Z_{13} = Z_{15} = Z_{17} = 0, \quad y = 0, \tag{2.17}$$
$$|\boldsymbol{Z}_1| \to 0, \quad y \to \infty,$$

The right-hand side of (2.17) is associated with non-parallel effects. Its explicit form coincides with that given in the Appendix of Fedorov & Khokhlov (2002) with the replacements: $\boldsymbol{F}_{k0} \to \boldsymbol{Z}_0$, $x_1 \to x_3$, $R \to R_\Lambda$ and $\alpha \to \tilde{\alpha}$.

A solution of the homogeneous problem (2.16) is expressed as

$$\boldsymbol{Z}_0 = C(x_3)\boldsymbol{\zeta}(x_3, y, \tilde{\alpha}), \tag{2.18}$$

where $\boldsymbol{\zeta}$ is the eigenvector normalized by the condition $\zeta_4(x_3, 0, \tilde{\alpha}) = 1$ (the wall pressure amplitude $= C(x_3)$). The inhomogeneous problem (2.17) has a non-trivial solution if its right-hand side is orthogonal to the eigenvector $\boldsymbol{\xi}(x_3, y, \tilde{\alpha})$ of the adjoint problem. This leads to the ordinary differential equation for the coefficient $C(x_3)$

$$\frac{\mathrm{d}C}{\mathrm{d}x_3} = WC, \tag{2.19}$$
$$W(x_3) = -\frac{\left\langle \boldsymbol{B}\dfrac{\partial \boldsymbol{\zeta}}{\partial x_3}, \boldsymbol{\xi} \right\rangle + \langle \boldsymbol{H}_1 \boldsymbol{\zeta}, \boldsymbol{\xi} \rangle}{\langle \boldsymbol{B}\boldsymbol{\zeta}, \boldsymbol{\xi} \rangle}, \quad \langle \boldsymbol{\zeta}, \boldsymbol{\xi} \rangle \equiv \int_0^\infty \sum_{j=1}^{8} \zeta_j \bar{\xi}_j \, \mathrm{d}y,$$

where $\boldsymbol{B} = -\mathrm{i}\partial \boldsymbol{H}_0 / \partial \tilde{\alpha}$, the overbar denotes a complex conjugate value. Equation (2.19) is supplemented with the initial condition resulted from matching of the inner expansion ($x_3 \to 0$) of the outer solution (2.18) with the outer expansion (2.11) ($x_2 \to +\infty$) of the inner solution (2.10). Performing this matching Fedorov & Khokhlov (1991, 1993) showed that there are two boundary-layer modes synchronized with the slow and fast acoustic waves near the leading edge ($x_3 \to 0$). Their eigenvalues are

$$\tilde{\alpha} = \alpha_{1,2} - \frac{k^2(\alpha_{1,2} - 1)^4}{2[M^2(\alpha_{1,2} - 1) - \alpha_{1,2}]} x_3 + \ldots, \quad x_3 \to 0. \tag{2.20}$$

Hereafter, the disturbance with $\tilde{\alpha} \to \alpha_1$ is called 'Mode S' (slow mode) and that with $\tilde{\alpha} \to \alpha_2$ 'Mode F' (fast mode). Near the leading edge, the pressure disturbance of these modes is expressed as

$$p = C_0 x_3^{1/4} \exp(\mathrm{i}\tilde{S}), \quad x_3 \to 0, \tag{2.21}$$
$$C_0 = \varepsilon^{-1/2}(\pi\lambda^2)^{1/8} E(q), \tag{2.22}$$

Case	M	T_0 (K)	T_w/T_{ad}	Δ
1	4.5	329	1	10.391
2	5.92	390	1	16.896
3	5.5	567.7	0.1	4.442

TABLE 1. The cases considered.

where λ and $E(q)$ are given by (2.9) and (2.12), respectively. In a similar way, the boundary-layer disturbance vector is

$$\boldsymbol{Z} = C_0 x_3^{1/4} \boldsymbol{\zeta}(x_3, y) \exp(\mathrm{i}\tilde{S}), \quad x_3 \to 0. \tag{2.23}$$

The relation (2.23) couples Modes S and F with an incident acoustic wave that solves the leading-edge receptivity problem for the case of small angles of incidence. Following the terminology of Goldstein (1983) we call C_0 the 'coupling coefficient'. Note that this coefficient does not depend on the longitudinal coordinate x_3.

It remains to be seen whether Modes S and F are relevant to unstable disturbances. This can be verified by integrating numerically the eigenvalue problem (2.16). Calculations are performed for air, which is treated as a perfect gas with Prandtl number 0.72 and specific heat ratio 1.4. The viscosity μ is approximated by the Sutherland formula; the second viscosity is $\mu_v = 0.8\mu$. The system of equations (2.16) is integrated from the boundary-layer edge to the wall using the fourth-order Runge–Kutta method with Gram–Schmidt orthonormalization to control the parasitic error growth. A Newton–Raphson procedure is used for the eigenvalue search. The integration domain contains 428 knots across the boundary layer which allows calculations of eigenvalues and eigenfunctions with the relative error less than 10^{-5}.

Hereafter we consider the cases listed in table 1: case 1 corresponds to the DNS of Ma & Zhong (2001); case 2 is relevant to the experiment of Maslov *et al.* (2001); case 3 exemplifies the boundary layer on a cooled plate. Figure 4(a,b) shows the eigenvalues of Modes S and F (solid lines) and their asymptotic approximations (2.20) (dashed lines) for two-dimensional waves ($\beta = 0$) of frequency $F = 5 \times 10^{-5}$ for case 2. The Reynolds number $R \equiv \sqrt{U_\infty^* x^*/\nu_\infty^*} = R_\Lambda \sqrt{x_3}/\Delta$ is also shown for reference. Despite the relatively large value of $\varepsilon = 0.304$, the numerical solutions (solid lines) of the full eigenvalue problem (2.16) are close to the asymptotic values (2.20) (dashed lines) for small x_3, especially for the real part of $\tilde{\alpha}$ shown in figure 4(a). The spatial growth rate, $-\mathrm{Im}(\tilde{\alpha})$, of Mode S has two maxima. The first maximum is located at relatively small x_3 and is associated with the first-mode instability according to the terminology of Mack (1969, 1987). The second maximum is relevant to the Mack second mode. Similar trends are observed for case 1. These cases are typical for hypersonic boundary layers on a thermally insulated (adiabatic) wall. They illustrate a situation when the unstable mode is synchronized with the slow acoustic wave near the leading edge. Results for case 3 in figure 5(a,b) are topologically different from those shown in figure (4a,b). Now, Mode F becomes unstable in the region $x_3 > 1$. This instability is again associated with the Mack second mode. Such a topology occurs in hypersonic boundary layers on cooled surfaces. A detailed analysis of these spectrum topologies and a criterion of switching from one topology to another are presented by Fedorov & Khokhlov (2001).

The numerical examples shown in figures 4 and 5 indicate that the terminology introduced by Mack (1969, 1987) to describe the multiplicity of inflectional neutral

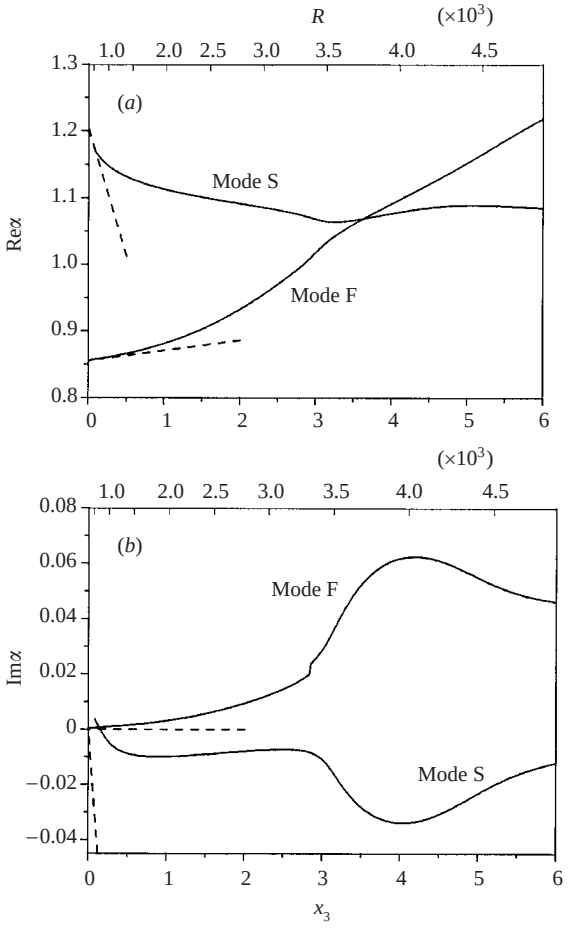

FIGURE 4. Eigenvalues $\alpha \equiv \tilde{\alpha}$ for case 2; two-dimensional disturbances of $F = 3 \times 10^{-5}$; $\varepsilon = 0.304$; solid lines, numerical solutions of (2.16); dashed lines, asymptotic relations (2.20).

modes becomes ambiguous when applied to non-neutral solutions, i.e. a single relation $\tilde{\alpha}(\omega)$ can be relevant to multiple 'higher-mode' solutions. This motivates us to associate the boundary-layer modes with their asymptotic behaviour near the leading edge and introduce Modes S and F, which are different from the Mack first and second modes.

2.4. *Scattering of acoustic waves at moderate angles of incidence*

Before considering disturbances with angles of incidence $\theta_y = O(1)$, we discuss the limit $q \to \infty$ relevant to $|\theta_y| \gg \varepsilon$. In this case, the right-hand side of (2.8) is expressed as

$$\exp(\pm \mathrm{i} q^2 x_2)[1 + q/|q|] - (\pm \mathrm{i}\pi x_2)^{-1/2}/q + \ldots. \tag{2.24}$$

Then, the function (2.12) can be decomposed into the two parts, $E = E_1 + E_2$, corresponding to the first and second terms of (2.24). Their asymptotic behaviours are

$$E_1 = E_0 \varphi(r)[1 + q/|q|] = O(q^{-2}), \quad q \to \infty, \tag{2.25}$$

$$E_2 = -E_0 \pi^{1/4} \sqrt{\pm\lambda/(\mathrm{i}\pi)}\,/(q A^2), \quad q \to \infty. \tag{2.26}$$

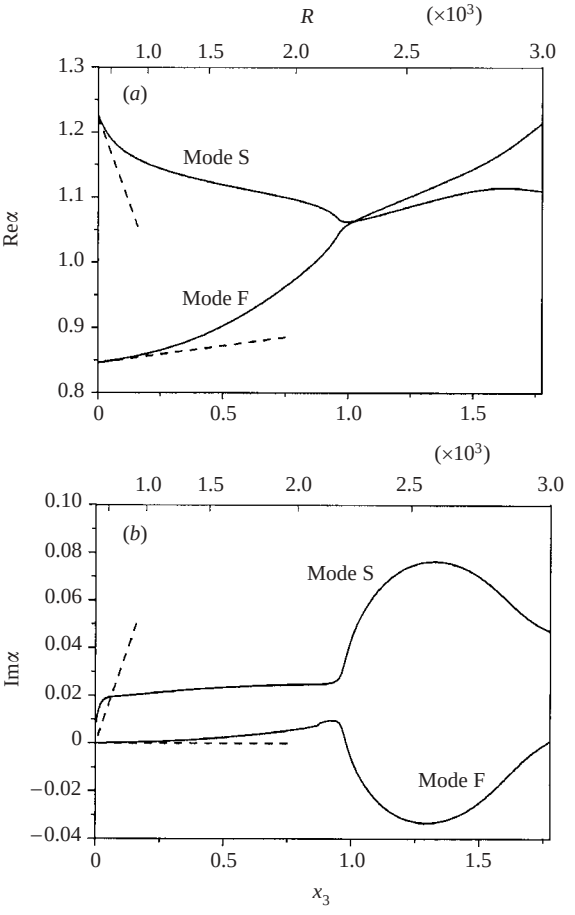

FIGURE 5. Eigenvalues $\alpha \equiv \tilde{\alpha}$ for case 3; two-dimensional disturbances of $F = 10^{-4}$; $\varepsilon = 0.211$; solid lines, numerical solutions of (2.16), dashed lines, asymptotic relations (2.20).

These relations indicate that two receptivity mechanisms become distinguishable as the angle of incidence increases:

(i) Mechanism (A) is associated with interaction of the incident and reflected waves with the non-parallel boundary-layer flow; it is governed by the term E_1.

(ii) Mechanism (B) is related to scattering of the incident wave by the leading edge; it is governed by the term E_2. The scattering induces a cylindrical acoustic source at the leading edge $x = 0$. The secondary acoustic field from this source, in turn, is synchronized with Modes S and F. The slow and fast acoustic waves generated by the leading-edge source are diffracted in the region $x_2 = O(1)$. This diffraction leads to excitation of Modes S and F similarly to the case of zero angle of incidence.

The relations (2.25)–(2.26) show that mechanism (B) becomes dominant as $q \to \infty$. This trend holds for relatively large angles of incidence θ_y relevant to significant deviations of the acoustic wavenumber α from $\alpha_{1,2}$.

For the angle of incidence $\theta_y = O(1)$, Fedorov & Khokhlov (1991, 1993) showed that the acoustic pressure in the scattering region $(x, y) = O(1)$ (see figure 3) is expressed as

$$p = p_0(x, y)\exp(\mathrm{i}\beta z - \mathrm{i}t) + O(\varepsilon^2), \tag{2.27}$$

where the amplitude p_0 has the following asymptotic behaviour over the upper surface of a flat plate

$$p_0 = 2\exp(\mathrm{i}\alpha x)\cos(\gamma y) + \sum_{j=1}^{2} G_j x^{-1/2}\exp(\mathrm{i}\alpha_j x) f_j(y/\sqrt{x}) + \ldots, \tag{2.28}$$

$$G_{1,2} = \mp \frac{\mathrm{i}\gamma(\alpha)\exp(\pm\mathrm{i}\pi/4)(\alpha_{1,2}-1)}{\sqrt{\pi(\alpha_1-\alpha_2)(M^2-1)}\,(\alpha_{1,2}-\alpha)(\alpha-1)}, \tag{2.29}$$

$$f_j(s) = \exp\{-\mathrm{i}s^2[M^2(\alpha_j-1)-\alpha_j]/2\}, \quad x \to +\infty, \quad y = O(x). \tag{2.30}$$

The first term of (2.28) represents incident and reflected acoustic waves in the upper half-plane $y > 0$. If the external wave is incident on the plate from below, this term must be omitted. The second part describes the secondary acoustic field from the leading-edge cylindrical source. Near the wall, this field is seen as slow ($\alpha = \alpha_1$) and fast ($\alpha = \alpha_2$) acoustic waves with their wave fronts perpendicular to the plate surface and their amplitudes slow functions of y. According to (2.28) the asymptotic expansions in the diffraction region $x_2 = O(1)$ are

$$p = \exp(\mathrm{i}S)\big[2\cos(\gamma y) + \varepsilon p_0^{(1)}(x_2, y) + O(\varepsilon^2)\big] + \varepsilon\big[\exp(\mathrm{i}\alpha_1 x + \mathrm{i}\beta z - \mathrm{i}t)p_1^{(1)}(x_2, y_2) + \exp(\mathrm{i}\alpha_2 x + \mathrm{i}\beta z - \mathrm{i}t)p_2^{(1)}(x_2, y_2)\big] + \ldots. \tag{2.31}$$

The term $p_0^{(1)}$ represents a small distortion of the reflected wave and contains no 'seed' for the boundary-layer modes. Its explicit form is $p_0^{(1)} = \mathrm{Const}\sqrt{x_2}\exp(-\mathrm{i}\gamma y)$. At the bottom of the diffraction layer $y_2 = 0$, the amplitudes $p_{1,2}^{(1)}$ are solutions of the integral equation

$$p_j^{(1)}(x_2) - \lambda \int_0^{x_2} \sqrt{\frac{\xi}{x_2-\xi}}\, p_j^{(1)}(\xi)\,\mathrm{d}\xi = G_j x_2^{-1/2}, \quad j = 1, 2. \tag{2.32}$$

This equation is similar to (2.8) derived for the case of small angles of incidence. The downstream asymptotic expression for $p_j^{(1)}$ contains an exponential term coinciding with the first term of (2.11) if the constant E_0 is replaced by the function

$$E(\alpha) = E_0 G_{1,2}\pi^{1/4}\lambda^{1/2}/A^2. \tag{2.33}$$

Mechanism (B) prevails over mechanism (A) for acoustic waves of $\theta_y = O(1)$. In this case the phase speeds of acoustic waves are significantly different from those of the boundary-layer modes. Such a detuning of the synchronization conditions weakens mechanism (A). On the other hand, the secondary acoustic field induced through mechanism (B) is always synchronized with Modes S and F. This feature may be examined by comparison of the boundary-layer responses to acoustic waves incident on the plate from above (figure 6*a*) and below (figure 6*b*). For the configuration shown in figure 6(*b*), mechanism (A) is not involved in the receptivity on the upper surface of the plate, since this surface is shielded from the incident wave. For the configuration shown in figure 6(*a*), both (A) and (B) contribute to the boundary-layer disturbance. Since the contributions from mechanism (B) are identical in both cases due to symmetry of scattering, the difference between the two signals measured at a certain point on the upper surface of plate characterizes effectiveness of mechanism (A).

Unfortunately, it is difficult to realize this situation experimentally because a real acoustic source generates entropy and vortical disturbances. If the source is above the

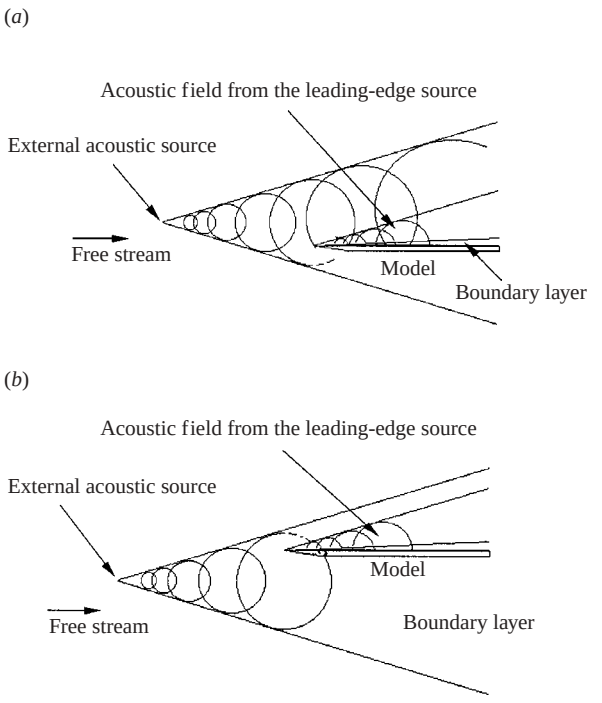

FIGURE 6. Schematics of boundary layer responses to acoustic waves incident on the plate from above (*a*) and below (*b*).

plate, the non-acoustic disturbances also contribute to the boundary-layer disturbance. Nevertheless, these disturbances can be filtered out by using wave trains instead of harmonic disturbances. Since the group velocities of the acoustic mode are essentially different from those of the entropy and vorticity modes, the external disturbances and corresponding responses of the boundary layer will be observed in different time intervals. Mechanisms (A) and (B) can also be examined by direct numerical simulations of the flow configurations shown in figure 6(*a*, *b*).

2.5. *Coupling coefficient*

For small angles of incidence relevant to $\alpha \to \alpha_{1,2}$, the source intensities $G_{1,2}$ given by (2.29) are singular. Fedorov & Khokhlov (1993) resolved this singularity by introducing the narrow regions $\alpha - \alpha_{1,2} = O(\varepsilon^2)$, where the inner solution is given by (2.12). The inner limit, $\alpha \to \alpha_{1,2}$, of the function $\varepsilon E(\alpha)$ (2.33) is matched with the outer limit, $q \to \infty$, of the function $E(q)$ (2.12). Then, (2.33) can be combined with (2.12) and expressed in the composite form

$$E_a(\alpha) = E_0[\varepsilon^{-1} P\,\psi(r) + \varphi(r)], \tag{2.34}$$

$$P \equiv \frac{\mathrm{i}\pi^{1/4}\gamma(\alpha)(\alpha_{1,2} - 1)\exp(\mp \mathrm{i}\pi/4)}{\lambda^{1/2}A^2(\alpha - 1)\sqrt{\pi(M^2 - 1)(\alpha_1 - \alpha_2)}}, \quad r = -\mathrm{i}(\alpha_{1,2} - \alpha)\varepsilon^{-2}(\pi\lambda)^{-1}. \tag{2.35}$$

Replacing $E(q)$ by $E_a(\alpha)$ in (2.22) we obtain the coupling coefficient for slow ($\alpha \geqslant \alpha_1$) and fast ($\alpha \leqslant \alpha_2$) acoustic waves of arbitrary angles of incidence:

$$C_0 = \varepsilon^{-1/2}(\pi\lambda^2)^{1/8} E_a(\alpha). \tag{2.36}$$

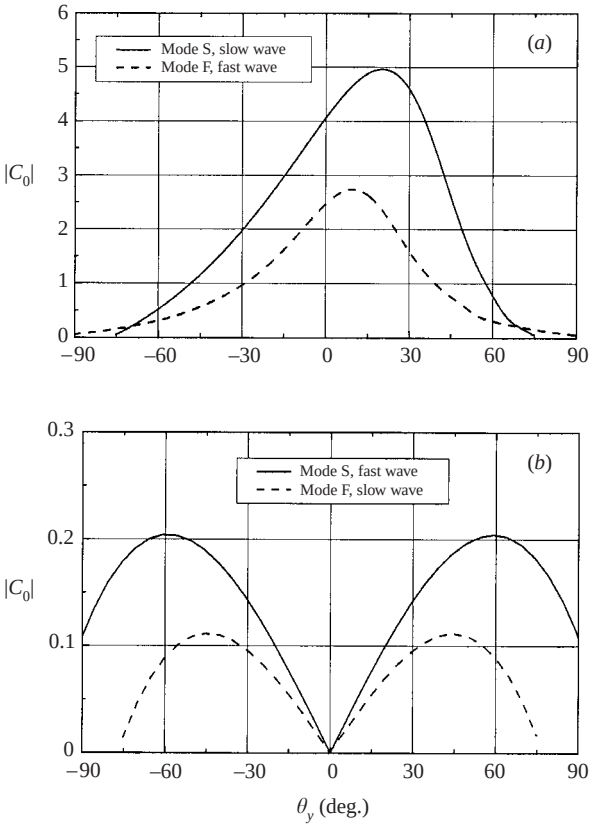

FIGURE 7. Coupling coefficient $|C_0|$ vs. incident angle θ_y; case 1, two-dimensional disturbances of $F = 5 \times 10^{-5}$; $\varepsilon = 0.271$.

Figures 7 and 8 illustrate parametric dependences of the coupling coefficient C_0. In figure 7(a,b) the modulus of $C_0(\theta_y)$ is show for two-dimensional waves ($\theta_z = 0$) for case 1 (table 1); the frequency parameter $F = 5 \times 10^{-5}$ and $\varepsilon = 0.271$. By definition Mode S (Mode F) is synchronized with the slow (fast) acoustic waves. Due to this synchronization Mode S (Mode F) is effectively generated by the slow (fast) wave, as shown in figure 7(a). Note that the coupling coefficients are not symmetric with respect to the angle of incidence. The maximum of $|C_0(\theta_y)|$ is observed at $\theta_y \approx 20°$ for Mode S and $\theta_y \approx 9°$ for Mode F, when both diffraction and scattering of the incident wave transfer energy to the boundary-layer mode. The excitation of Mode S (Mode F) via the fast (slow) wave is an order of magnitude weaker, as shown in figure 7(b). In this case, the receptivity process involves mechanism (B) only. Since the acoustic-wave scattering is antisymmetric with respect to θ_y, the coupling-coefficient modulus is an even function. At the angle of incidence $\theta_y = 0$, there is no scattering and mechanism (B) gives $C_0 = 0$ in the dominant-order approximation.

The coupling coefficient of Mode S is shown in figure 8(a,b) at various sweep angles θ_z. For slow acoustic waves, $|C_0(\theta_y)|$ monotonically increases with θ_z. For fast waves, $|C_0(\theta_y)|$ decreases with θ_z for $\theta_y < 84°$ and increases for $\theta_y > 84°$. This non-monotonic behaviour is due to competition between the two trends: decreasing of the $|C_0(\theta_y)|$ maximum and widening of the θ_y range as θ_z increases. Similar trends are observed in cases 2 and 3, which are not illustrated here.

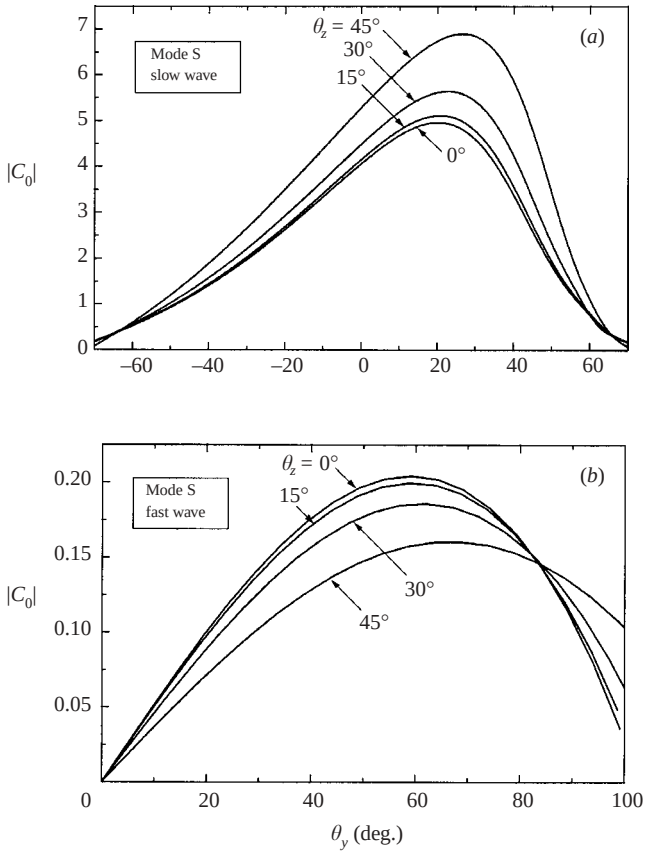

FIGURE 8. Coupling coefficients $|C_0(\theta_y)|$ for various sweep angles θ_z; case 2, two-dimensional disturbances of $F = 5 \times 10^{-5}$; $\varepsilon = 0.271$.

2.6. *Comparison with experiment*

Maslov *et al.* (2001) performed experimental studies of the leading-edge receptivity to acoustic waves induced by two-dimensional and three-dimensional actuators. The experiments were conducted in a hypersonic blow-down wind tunnel at $M = 5.92$ and the unit Reynolds number $Re_1 = U^*_\infty/\nu^*_\infty = 13 \times 10^6$ m^{-1}. The experimental setup comprises a flat plate with an actuator and a test plate. Both plates have sharp leading edges. A glow-discharge actuator generates acoustic waves of a fixed frequency, which are incident on the leading edge of the test plate from below.

The α- and β-spectra of the longitudinal mass-flow disturbances were measured just in front the leading edge of the test plate using a hot-wire anemometer. These data provide the mass-flow amplitudes $Q_a(X = 0)$ of acoustic waves incident on the test plate. Measurements of the boundary-layer disturbances Q_{bl} on the test plate were conducted at a fixed distance ΔX from its leading edge. The hot wire was positioned at the location of maximum mass-flow fluctuations across the boundary layer. The receptivity coefficient was determined as

$$K(\alpha, \beta, \Delta X) = Q_{bl}(\alpha, \beta)_{X=\Delta X} / Q_a(\alpha, \beta)_{X=0}, \tag{2.37}$$

where both α and β refer to wavenumbers of the incident acoustic wave. Using the x-momentum equation and the energy equation for acoustic disturbances in

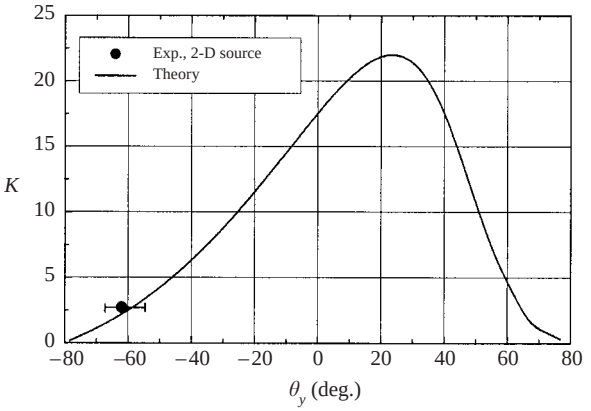

FIGURE 9. Receptivity coefficient for case 2; $M = 5.92$, two-dimensional disturbances of $F = 3 \times 10^{-5}$.

uniform compressible flow, we obtain the relationship between the mass-flow and pressure amplitudes $Q_a = [M^2 - 1/(1-c)]p$, where the phase speed is $c = 1/\alpha$ with α given by (2.5). The mass-flow disturbance in the boundary layer is determined from the eigenvector $\boldsymbol{\zeta}(x_3, y)$ of the corresponding boundary-layer mode at station $x^* = \Delta X$. It is expressed as $q(x_3, y) = [\zeta_1 + U(\gamma M^2 \zeta_4 - \zeta_5/T)]/T$, where the eigenvector is normalized by the condition $\zeta_4(x_3, 0) = 1$. Then the receptivity coefficient (2.37) is written in the form

$$K = \left| \frac{q_m(x_3)}{[M^2 - 1/(1-c)]} C_0 x_3^{1/4} \exp(\mathrm{i}\tilde{S}) \right|, \tag{2.38}$$

where $q_m(x_3) = \max_y q(x_3, y)$, x_3 and $\tilde{S}(x_3)$ are calculated at $x^* = \Delta X$; the coupling coefficient C_0 is given by (2.36).

2.6.1. *Two-dimensional actuator*

For a two-dimensional actuator with frequency $F = 3 \times 10^{-5}$ the acoustic wave in the leading-edge vicinity had the phase speed $c \approx 0.64$ corresponded to the slow wave of $\theta_y \approx -62°$, $\theta_z = 0$. The boundary-layer disturbance was measured at station $\Delta X = 10$ mm where $R = \sqrt{U_\infty^* \Delta X / \nu_\infty^*} = 360.5$ and $x_3 = 2 \times 10^{-3}$. For such a small value of x_3, the exponential term in (2.38) is approximated as $|\exp(\mathrm{i}\tilde{S}(x_3))| = 1$. Calculations of the receptivity coefficient for Mode F show that its value is an order of magnitude smaller than that for Mode S. Moreover, the phase measurements in the boundary layer on the test plate gives the phase speed $c \approx 0.85$, which is very close to the theoretical value $c = 0.849$ for Mode S. This allows us to ignore the contribution of Mode F into the boundary-layer disturbance. Figure 9 shows the receptivity coefficient K calculated for Mode S as a function of θ_y. The experimental value is shown by the symbol with the error bar indicating uncertainty of measurements. The theoretical prediction is remarkably close to the experimental point.

2.6.2. *Three-dimensional actuator*

The phase measurements showed that the phase speed of acoustic waves generated by a three-dimensional actuator was constant with accuracy of 10% for all sweep angles θ_z. The disturbance with frequency $F = 3 \times 10^{-5}$ had phase speed $c \approx 1.83$ corresponding to fast acoustic waves. The receptivity coefficients were measured at station $\Delta X = 20.1$ mm ($R = 511$ and $x_3 = 4 \times 10^{-3}$).

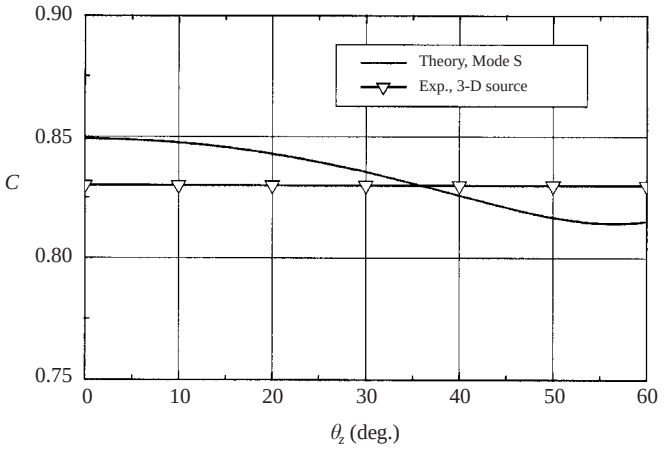

FIGURE 10. Phase speed of boundary-layer disturbance at $\Delta X = 20.1\,\text{mm}$, $F = 3 \times 10^{-5}$.

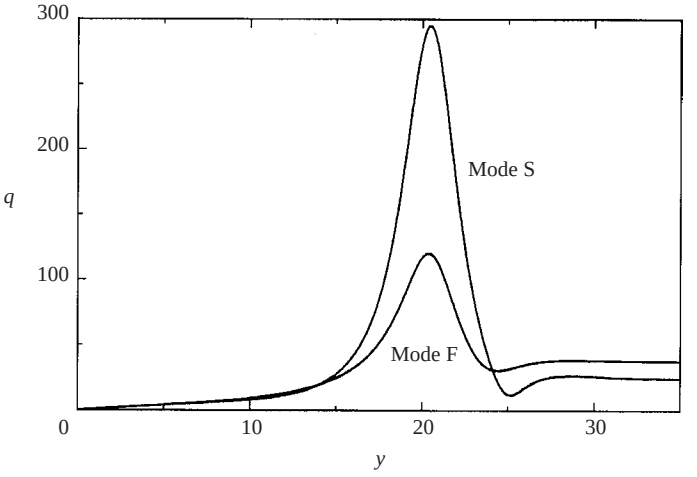

FIGURE 11. Mass-flux distributions for Modes S and F at $\Delta X = 20.1\,\text{mm}$, $F = 3 \times 10^{-5}$.

Figure 10 shows that the phase speed calculated for Mode S is close to the experimental value $c \approx 0.83$, i.e. Mode S is expected to make the dominant contribution to the boundary-layer disturbance. At first glance, this contradicts the conclusion of § 2.5 that fast acoustic waves predominantly generate Mode F. To clarify this issue we performed receptivity calculations for both Mode S and Mode F in the range $0 \leqslant \theta_z \leqslant 60°$. It turned out that the coupling coefficient C_0(Mode S, fast waves) is of the order of C_0(Mode F, fast waves) due to relatively high angles of incidence, $\theta_y \approx -70°$. This is consistent with the data shown in figures 7 and 8. In addition, the mass-flow maximum q_m(Mode S) is significantly larger than q_m(Mode F) as shown in figure 11. This leads to the ratio K(Mode S)/K(Mode F) > 3 for $0° \leqslant \theta_z \leqslant 60°$, i.e. the excitation of Mode S by fast acoustic waves is, indeed, dominant in the case considered. This allows us to assume that the experimental receptivity coefficients are predominantly related to Mode S.

Figure 12 shows K(Mode S) as a function of θ_y for two-dimensional waves ($\theta_z = 0$). The experimental point (symbol) is again very close to the theoretical curve. In

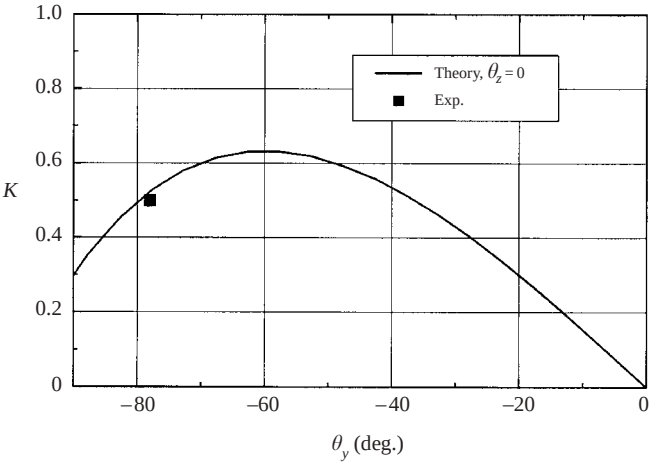

FIGURE 12. Receptivity coefficient for Mode S vs. incident angle; $\Delta X = 20.1$ mm, $F = 3 \times 10^{-5}$.

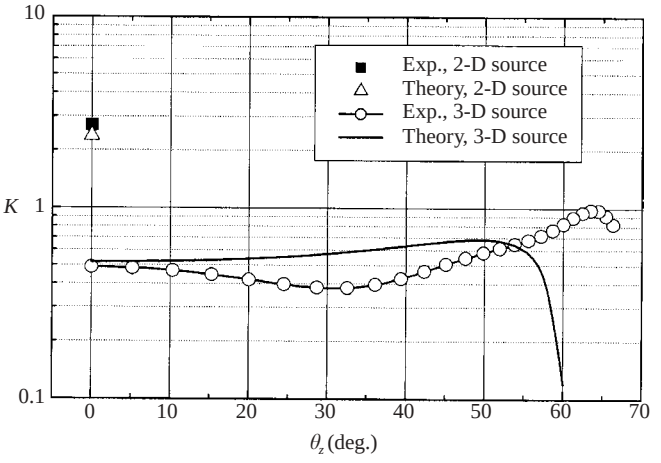

FIGURE 13. Receptivity coefficients for Mode S vs. sweep angle, $F = 3 \times 10^{-5}$; $c = 0.64$ for two-dimensional source; $c = 1.83$ for three-dimensional source.

figure 13, the theoretical predictions and the experimental data are shown for various sweep angles θ_z. The data for to the two-dimensional source are also presented for comparison. Notwithstanding the difficult conditions for theoretical modelling (high angles of incidence and relatively large value of the small parameter $\varepsilon \approx 0.3$) as well as large uncertainty in the experimental data (about 20% for K), good agreement is observed in the range $0 \leqslant \theta_z < 50°$. For higher sweep angles, the theoretical and experimental curves diverge significantly. This discrepancy may be due to the uncertainty in the experimental data, which strongly increases with θ_z. Another reason is associated with the fact that the theoretical model needs to be revised for large θ_z. As the sweep angle approaches its limiting value $\cos^{-1}(1/M)$, the wavenumber α_1 given by (2.4) tends to infinity, whereas the phase speed $c_1 = 1/\alpha_1 \to 0$ and the critical point $y_c \to 0$. Ultimately the critical layer merges with the Stokes layer, which leads to a new asymptotic structure in the near-field boundary layer at

$x_2 = O(1)$. This appears to be the triple-deck structure, which is extensively used for theoretical modeling of TS waves (Smith 1989; Kozlov & Ryzhov 1990).

Maslov *et al.* (2001) also reported receptivity data for acoustic wave components with negative phase speeds: $c \approx -0.75$ and $c \approx -1.48$. In these cases, the leading edge of the test plate is very close to the conical envelope of acoustic wave fronts radiated from a three-dimensional source. In the vicinity of this envelope, which can be treated as an unsteady three-dimensional shocklet, the acoustic field is highly non-uniform and its amplitude is significantly larger than that observed within the acoustic cone. The receptivity problem for this configuration appears to be associated with interaction of unsteady shocklets with the plate leading edge, which is beyond the scope of this paper.

3. Inter-modal exchange

3.1. *Problem formulation*

The DNS of Ma & Zhong (2001) showed that two-dimensional fast acoustic waves of zero angle of incidence ($\theta_y = 0$, $\theta_z = 0$) were able to generate Mode S in the boundary layer on a flat plate with a sharp leading edge. The numerical simulation was performed for case 1 of table 1. The asymptotic model of § 2 fails to predict this result because the coupling coefficient is zero in the dominant-order approximation (see figure 7*b*). To address this case one needs to identify additional mechanisms transferring energy to Mode S somewhere downstream from the leading edge.

Such a mechanism may be associated with the inter-modal exchange discussed by Fedorov & Khokhlov (1993, 2001). With this assumption Mode F is generated by the fast acoustic wave near the leading edge. Then, Mode F excites Mode S due to non-parallel effects. Since the phase speeds of Modes S and F are close to each other (see Region 3 in figure 1), even a weak non-uniformity of the mean flow may lead to significant interactions between the modes.

The inter-modal exchange can be modelled using the multiple-mode method developed by Zhigulev, Sidorenko & Tumin (1980) for incompressible boundary layers and extended by Tumin & Fedorov (1983) to compressible flows. This method was also described by Zhigulev & Tumin (1987) and Fedorov & Khokhlov (2001, 2002). Next, we briefly outline its basic elements.

The disturbance vector (2.14) is expressed as the eigenfunction decomposition

$$\boldsymbol{Z} = \sum_{\alpha} C_\alpha(x_3)\boldsymbol{\zeta}_\alpha(x_3, y)\exp[\mathrm{i}\tilde{S}_\alpha(x_3)], \quad \tilde{S}_\alpha(x_3) = \varepsilon^{-4}\int_{x_{30}}^{x_3} \tilde{\alpha}\,\mathrm{d}x_3 + \beta z - t, \tag{3.1}$$

where $\sum_\alpha$ denotes summation over the discrete spectrum and integration over continuous spectra. The amplitude coefficients $C_\alpha(x_3)$ are solutions of the ordinary differential equations

$$\frac{\mathrm{d}C_\alpha}{\mathrm{d}x_3} = \sum_{\gamma} C_\gamma(x_3) W_{\alpha\gamma}(x_3)\exp[\mathrm{i}(\tilde{S}_\gamma - \tilde{S}_\alpha)], \tag{3.2}$$

$$W_{\alpha\gamma} = -\frac{\left\langle \boldsymbol{B}\dfrac{\partial \boldsymbol{\zeta}_\gamma}{\partial x}, \boldsymbol{\xi}_\alpha \right\rangle + \langle \boldsymbol{H}_1\boldsymbol{\zeta}_\gamma, \boldsymbol{\xi}_\alpha\rangle}{\langle \boldsymbol{B}\boldsymbol{\zeta}_\alpha, \boldsymbol{\xi}_\alpha\rangle}. \tag{3.3}$$

Equations, (3.2)–(3.3) appear to be an extension of (2.19) to the multi-modes case. The diagonal elements $W_{\alpha\alpha}$ describe non-parallel effects on the evolution of a single mode.

The non-diagonal elements $W_{\alpha\gamma}$ represent an interaction between different modes. If one of these modes belongs to the continuous spectrum, then $W_{\alpha\gamma}$ couples the external disturbances with the boundary-layer modes (receptivity problem). If both modes belong to the discrete spectrum, the matrix elements represent the inter-modal exchange. If the mean flow is parallel, then all matrix elements $W_{\alpha\gamma} = 0$ and no coupling occurs between modes.

3.2. *Comparison with DNS*

An exchange between Modes S and F is modelled using the two-mode approximation

$$\boldsymbol{Z} = C_1\boldsymbol{\zeta}_1(x_3, y)\exp(\mathrm{i}\tilde{S}_1) + C_2\boldsymbol{\zeta}_2(x_3, y)\exp(\mathrm{i}\tilde{S}_2), \tag{3.4}$$

where the subscripts 1 and 2 denote Modes S and F, respectively. The initial amplitudes are specified using the leading-edge receptivity model of § 2 as

$$x_3 \to 0: \quad C_1 \to C_0^{(1)} x_3^{1/4}\exp(\mathrm{i}\tilde{S}_1), \quad C_2 \to C_0^{(2)} x_3^{1/4}\exp(\mathrm{i}\tilde{S}_2), \tag{3.5}$$

where the coupling coefficients $C_0^{(1,2)}$ are calculated using (2.36).

The system of equations (3.2) with the initial conditions (3.5) was integrated numerically using the fourth-order Runge–Kutta method. The integration domain contains more than 2000 knots, which allows computations of the disturbance amplitude with relative error less than 10^{-3}.

Calculations were conducted for case 1 of table 1 corresponding to the DNS of Ma & Zhong (2001). To be consistent with the DNS data, hereafter we use the Reynolds number $R \equiv \sqrt{U_\infty^* x^*/\nu_\infty^*}$ as a streamwise variable. Then the wavenumber is expressed as $\alpha \equiv \alpha^*\sqrt{\nu_\infty^* x^*/U_\infty^*} = \tilde{\alpha} R F$. The fast acoustic wave has the frequency $F = 2.2 \times 10^{-4}$ and the angles $\theta_y = \theta_z = 0$. For this set of parameters, the leading-edge receptivity model gives $C_0^{(1)} = 0$ and $C_0^{(2)} \neq 0$, i.e. the fast wave generates Mode F only.

In figure 14(a,b) the eigenvalues of Modes S and F are shown as functions of R. While the real parts $\mathrm{Re}[\alpha_{1,2}(R)]$ are very close to each other at $R \approx 900$, the imaginary parts $\mathrm{Im}[\alpha_{1,2}(R = 900)]$ are different. The synchronization point R_s, resulting from the condition $\alpha_1 = \alpha_2$, is essentially complex and so may lead to distributed rather than local inter-modal exchange. This conjecture is confirmed by the data presented in figures 15–17.

Figures 15(a) and 15(b) show distributions of the wall pressure amplitude for Modes S and F respectively. Different curves represent solutions for different initial points $R_0 = \sqrt{U_\infty^* x_0^*/\nu_\infty^*}$. The amplitude of Mode F weakly depends on R_0, i.e. the initial condition is captured well by the asymptotic relation (3.5). On the other hand, the amplitude of Mode S mainly depends on the initial point. This effect is illustrated in figure 16, where the wall pressure amplitude at the upper neutral branch, $R = 988$, is plotted as a function of R_0. The solid line shows the amplitude of the unstable Mode S and symbols show the amplitude of Mode S plus Mode F. The slope of this distribution can be treated as the strength of the inter-modal exchange. The solution of (3.2)–(3.5) is dominated by the initial boundary rather than by the phase synchronization in the vicinity of $R = 900$ (see figure 14).

The disturbance amplitude approaches the DNS prediction of Ma & Zhong (2001) as the initial point decreases. This allows us to conclude that the two-mode approximation captures qualitative features of the receptivity process. However, quantitative agreement is poor because the disturbance frequency is relatively high and the asymptotic regions are not distinguished.

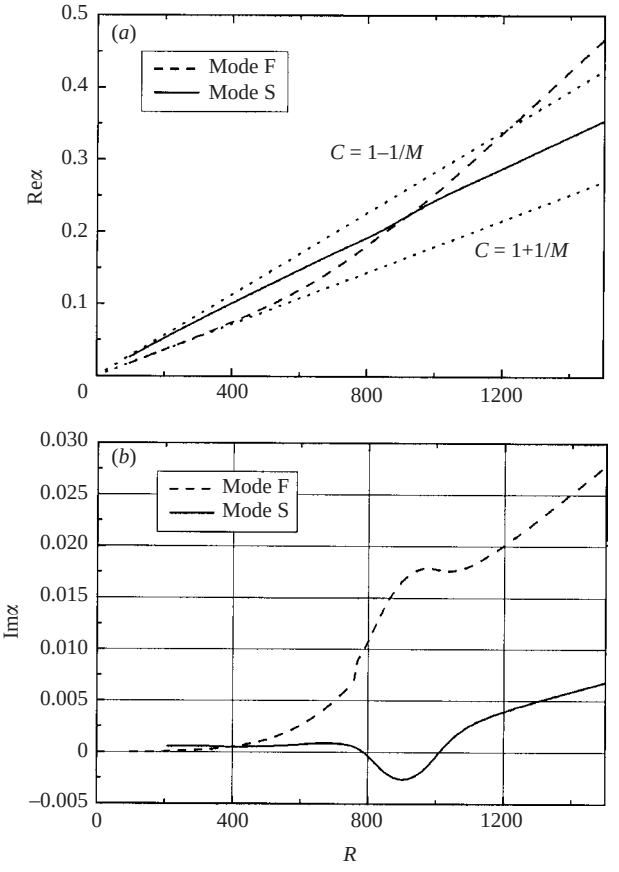

FIGURE 14. Eigenvalues $\alpha \equiv \tilde{\alpha} RF$ of Modes S, F and wavenumbers of the fast and slow acoustic waves for case 1: $M = 4.5$, two-dimensional disturbances of $F = 2.2 \times 10^{-4}$.

3.3. *Inter-modal exchange against leading-edge receptivity*

Figure 17 shows the wall pressure distributions $p_w(R) = |p_1 + p_2|$ of Mode S plus Mode F excited by the slow and fast acoustic waves. The leading-edge receptivity to the slow acoustic wave (dashed line) is significantly stronger than that resulting from the distributed inter-modal exchange (solid line). This case illustrates the disturbance dynamics of weakly unstable Mode S with the instability region not very far from the leading edge.

More practical situations involve disturbances of lower frequencies, when the amplification ratio is $\sim 10^3 - 10^4$. In these cases, it is difficult to perform DNS and wind-tunnel experiments because of the high Reynolds numbers. On the other hand, the combined numerical and asymptotic approach works better and provides higher accuracy at larger R and smaller F. As an example, we consider disturbances of frequency $F = 5 \times 10^{-5}$ with the other parameters being the same as in the case shown in figures 14–17. The eigenvalues of Modes S and F are shown in figure 18. Mode S is weakly unstable in the region $590 < R < 2450$ associated with two-dimensional disturbances of the first mode. Then, Mode S becomes highly unstable in the region $3640 < R < 4580$ related to instability of the second mode. Mode F is almost neutral in the upstream region $R < 3000$ and highly stable in the region of the second-mode instability.

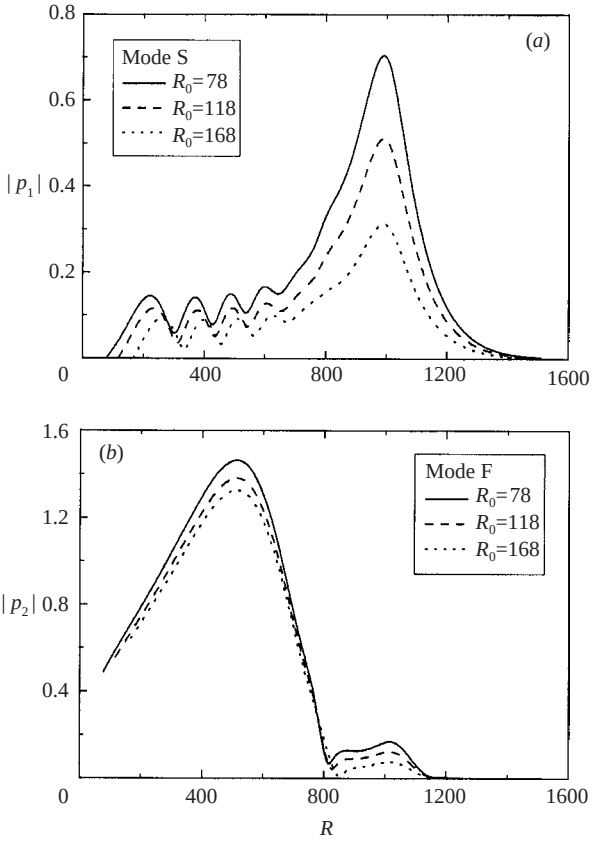

FIGURE 15. Wall pressure amplitudes of (*a*) Mode S and (*b*) Mode F for case 1: $M = 4.5$, two-dimensional disturbances of $F = 2.2 \times 10^{-4}$.

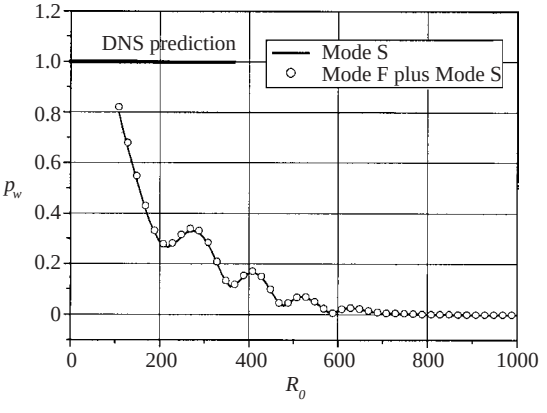

FIGURE 16. The wall pressure amplitude at the upper neutral branch as a function of the initial point R_0 and the DNS prediction of Ma & Zhong (2001); case 1, two-dimensional disturbances of $F = 2.2 \times 10^{-4}$.

Figure 19*a* (19*b*) shows the wall pressure amplitude $p_w = |p_1 + p_2|$ of Mode S plus Mode F for excitation by the fast (slow) acoustic wave with angles $\theta_y = \theta_z = 0$. Arrows indicate the initial point R_0. The solution is sensitive to R_0 in the case of excitation by

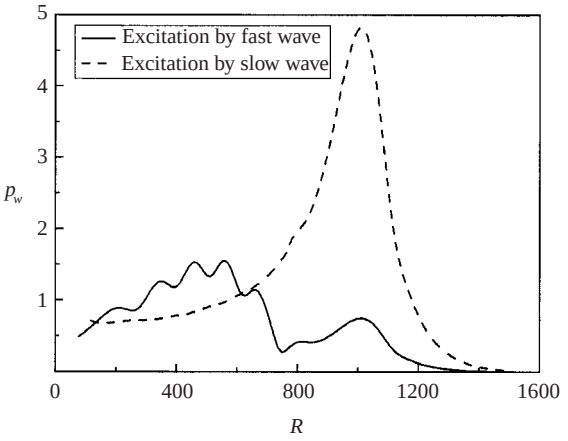

FIGURE 17. The wall pressure disturbance of Mode S plus Mode F excited by fast and slow acoustic waves; case 1, two-dimensional disturbances of $F = 2.2 \times 10^{-4}$.

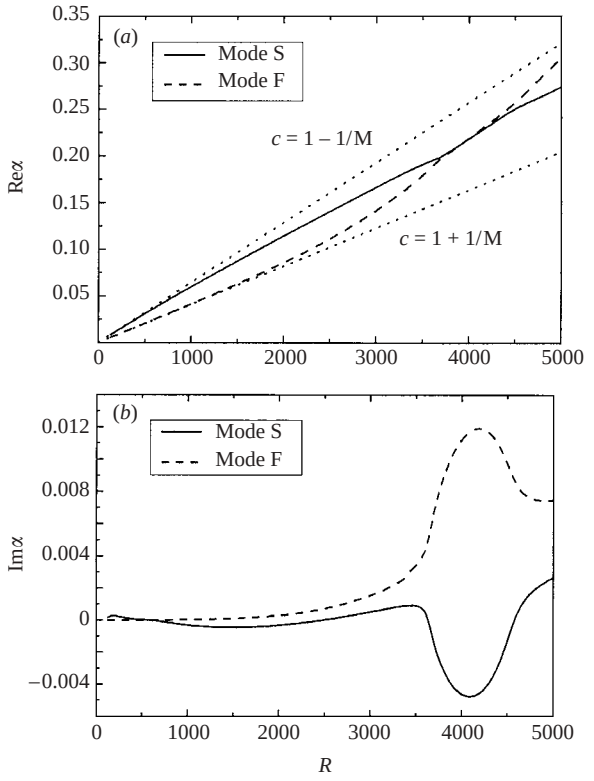

FIGURE 18. Eigenvalues $\alpha \equiv \tilde{\alpha} RF$ of Modes S, F and wavenumbers of the fast and slow acoustic waves for case 1; two-dimensional disturbances of $F = 5 \times 10^{-5}$.

the fast acoustic wave, when the unstable Mode S is predominantly generated via the distributed interaction with Mode F. On the other hand, the disturbance amplitude relevant to excitation by the slow acoustic wave weakly depends on the initial point, indicating that the leading-edge receptivity is stronger than the inter-modal exchange.

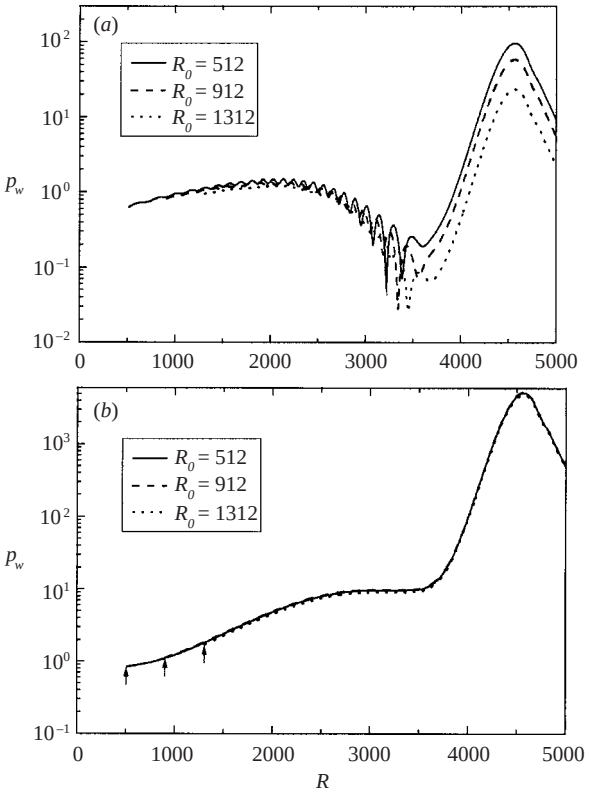

FIGURE 19. The wall pressure disturbance of Mode S plus Mode F excited by (*a*) fast and (*b*) slow acoustic waves; case 1, two-dimensional disturbances of $F = 5 \times 10^{-5}$.

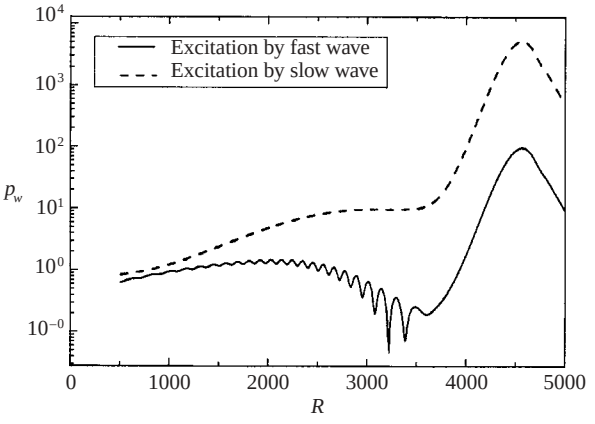

FIGURE 20. The wall pressure disturbance of Mode S plus Mode F excited by fast and slow acoustic waves; case 1, two-dimensional disturbances of $F = 5 \times 10^{-5}$.

As shown in figure 20, the direct excitation of Mode S by the slow acoustic wave (dashed line) yields an amplitude maximum approximately 50 times larger than that resulting from the inter-modal exchange (solid line).

The examples shown in figures 17 and 20 indicate that the leading-edge receptivity is stronger than the inter-modal exchange for a boundary layer on an adiabatic

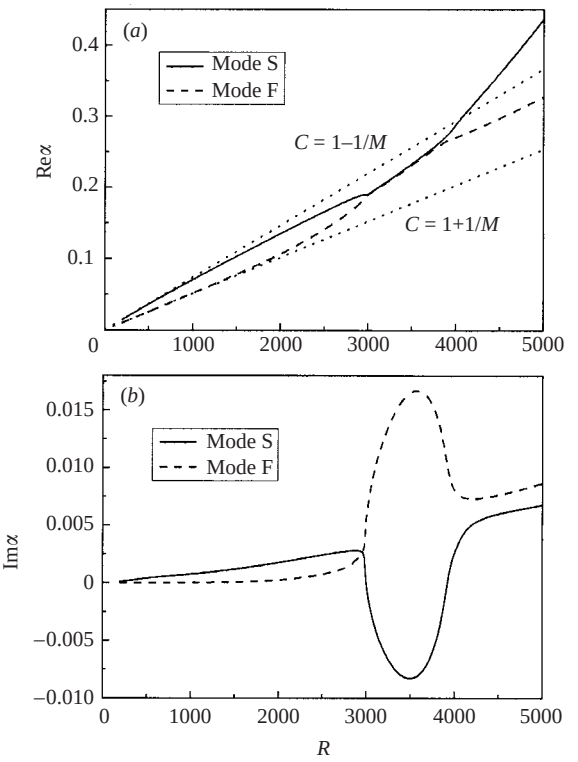

FIGURE 21. Eigenvalues $\alpha \equiv \tilde{\alpha} RF$ of Modes S, F and wavenumbers of the fast and slow acoustic waves for $M = 5.5$, $T_0 = 567.7\,\mathrm{K}$, $T_w = 1.5$; two-dimensional disturbances of $F = 6 \times 10^{-5}$.

wall. However, this balance may be different in the case of cooled walls. Fedorov & Khokhlov (1993, 2001) showed that the synchronization point R_s may be very close to the real axis at sufficiently small wall temperatures T_w. This may intensify the local interaction of Modes S and F in the vicinity of the synchronization point and change the relation between the leading-edge receptivity and the inter-modal exchange. Such a situation is exemplified by the disturbance spectrum shown in figure 21 for the case of $M = 5.5$, $T_w = 1.5$ ($T_w/T_{ad} \approx 0.25$), $T_0 = 567.7\,\mathrm{K}$ and $F = 6 \times 10^{-5}$, with the synchronization point $R_s \approx 2960$ being close to the neutral point $R = 3000$ of Mode S. Distributions of the wall pressure amplitude $p_w = |p_1 + p_2|$ calculated at various initial points R_0 are plotted in figure 22*a* (22*b*) for excitation by the slow (fast) acoustic wave; arrows indicate the initial points.

As shown in figure 22(*a*), the slow acoustic wave generates Mode S of amplitude ~ 1 near the leading edge. This mode attenuates downstream and reaches the neutral point with the relatively small amplitude $\sim 10^{-2}$. Its further amplification leads to a maximum amplitude of the order of 10^3 at the upper neutral branch $R = 3950$. In this case, the inter-modal exchange plays a minor role in the receptivity process.

For excitation by the fast acoustic wave (figure 22*b*), the disturbance behaviour is quite different. Mode F is generated near the leading edge and reaches the synchronization region with the amplitude ~ 1. Then, Mode F generates the unstable Mode S of amplitude ~ 1 via the inter-modal exchange in the vicinity of the synchronization point R_s. Further downstream, Mode S exponentially grows to amplitude $\sim 10^5$ at $R = 3950$. The role of inter-modal exchange is clearly shown

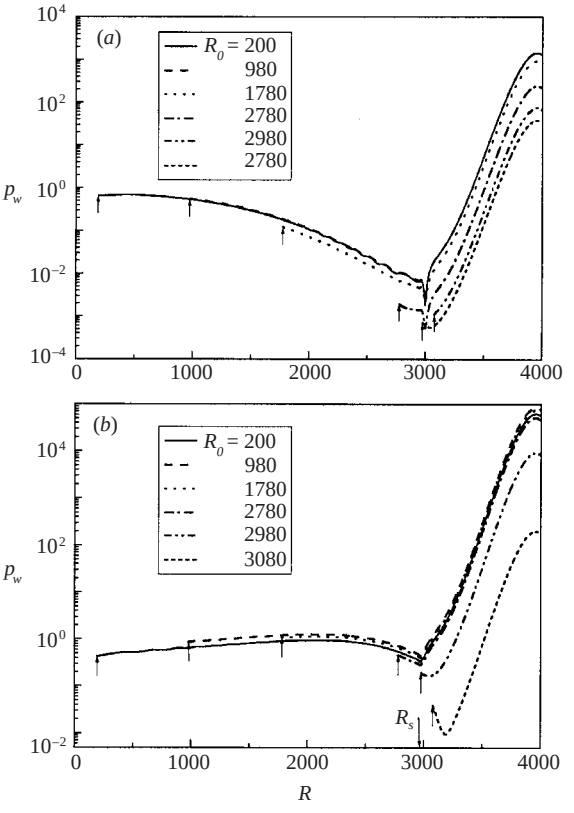

FIGURE 22. The wall pressure disturbance of Mode S plus Mode F excited by (*a*) slow and (*b*) fast acoustic waves for $M = 5.5$, $T_0 = 567.7\,\mathrm{K}$, $T_w = 1.5$; two-dimensional disturbances of $F = 6 \times 10^{-5}$.

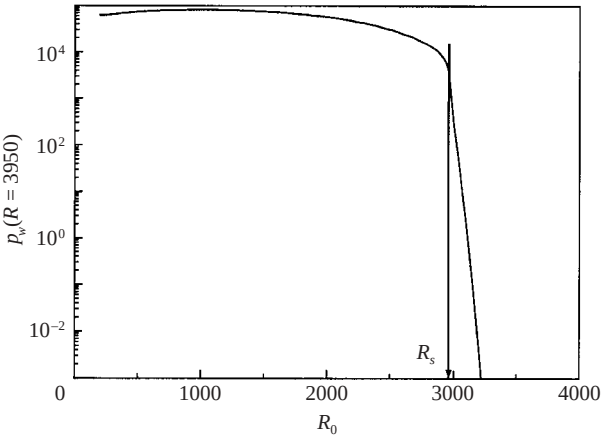

FIGURE 23. The wall pressure amplitude at the upper neutral branch as a function of the initial point R_0 for $M = 5.5$, $T_0 = 567.7\,\mathrm{K}$, $T_w = 1.5$; two-dimensional disturbances of $F = 6 \times 10^{-5}$.

in figure 23, where the maximum amplitude $p_w(R = 3950)$ is plotted as a function of the initial point R_0. The solution is weakly sensitive to the initial point until the latter is far upstream of the synchronization point R_s. As R_0 crosses R_s, the disturbance

amplitude sharply decreases. Comparing the disturbance amplitude given by solid lines in figure 22(a, b) we conclude that excitation of Mode S by the fast acoustic wave via the local inter-modal exchange is stronger than that by the slow acoustic wave via the leading-edge receptivity.

4. Concluding remarks

The receptivity of a high-speed boundary layer on a flat plate to acoustic disturbances has been modelled using a combination of asymptotic and numerical methods. It was shown that acoustic waves are synchronized with the first and second boundary-layer modes in the vicinity of the leading edge. This property of the disturbance spectrum leads to a new asymptotic structure of the disturbance field and causes significant changes in the coupling coefficient compared with the subsonic boundary layer.

The leading-edge receptivity is associated with scattering and diffraction of acoustic disturbances. Interplay of these effects depends mainly on the angle of incidence θ_y:

(i) For $\theta_y = 0$ (the acoustic wave front is normal to the plate surface), a dominant mechanism is diffraction of the incident acoustic wave due to the boundary-layer growth. This leads to a partial translation of acoustic disturbances to the boundary-layer modes, namely, Modes S and F.

(ii) For $\theta_y < 0$ (acoustic wave incident on the leading edge from below the measurement side), scattering of the incident wave leads to a cylindrical source concentrated at the leading edge. This source induces the secondary acoustic field, which is synchronized with the boundary-layer modes and effectively generates the latter via the diffraction mechanism similarly to case i).

(iii) For $\theta_y > 0$ (acoustic wave incident on the leading edge from above the measurement side), both scattering and diffraction are involved in the receptivity process.

The leading-edge receptivity theory agrees well with the experimental data of Maslov *et al.* (2001) obtained in a Mach 6 wind tunnel on a flat plate with a sharp leading edge. The theoretical receptivity coefficient for two-dimensional acoustic waves is remarkably close to the experimental data point. Good agreement is also observed for three-dimensional acoustic waves in the sweep angle range $0 \leqslant \theta_z < 50^\circ$. For larger θ_z, the theoretical and experimental curves diverge since the disturbance field changes its asymptotic structure, which seems to become the triple-deck structure associated with oblique TS waves (Smith 1989) rather than the second-mode instability.

The unstable boundary-layer mode can also be excited downstream from the leading edge via the inter-modal exchange due to non-parallel effects. This mechanism has been modelled using the multiple-modes method, namely its two-mode approximation. A combination of the leading-edge receptivity theory with the two-mode approximation captures qualitative features of the direct numerical simulation of Ma & Zhong (2001). However, quantitative agreement is poor because the disturbance frequency is relatively high and the asymptotic regions are not distinguished.

It has been shown that the distributed inter-modal exchange is significantly weaker than the local leading-edge receptivity for the boundary layer on an adiabatic wall. However, the inter-modal exchange becomes dominant in the case of pure synchronization between the boundary-layer modes. This situation occurs in high-speed boundary layers on cooled walls, when the discrete spectrum has its synchronization point close to the real parameter space. The relationship between the leading-edge receptivity and the inter-modal exchange strongly depends on the location of the

synchronization point, which, in turn, is a function of mean-flow parameters and disturbance frequency. Both mechanisms should be taken into account for accurate prediction of the disturbance amplitude.

The present study shows that a combination of asymptotic and numerical methods provides a robust tool for receptivity modelling. This approach helps to identify basic mechanisms of the receptivity process and enables a comparative analysis. It may also guide further DNS and experimental studies of boundary-layer receptivity at supersonic and hypersonic speeds.

The author acknowledges Professor Anatoly Maslov and Dr Alexander Shiplyuk who kindly provided details on the leading-edge receptivity experiment. Parts of this work were supported by European Office of Aerospace Research and Development, Project SPC-98-4071, and INTAS, Grant 2000-0007.

REFERENCES

Choudhari, M. 1994 Theoretical prediction of boundary-layer receptivity. *AIAA Paper* 94-2223.

Choudhari, M. 1996 Boundary-layer receptivity to three-dimensional unsteady vortical disturbances in free stream. *AIAA Paper* 96-0181.

Choudhari, M. & Streett, C. 1990 Boundary layer receptivity phenomena in three-dimensional and high-speed boundary layers. *AIAA Paper* 90-5258.

Fedorov, A. V. & Khokhlov, A. P. 1991 Excitation of unstable modes in a supersonic boundary layer by acoustic waves. *Fluid Dyn.* No. 9, 456–467.

Fedorov, A. V. & Khokhlov, A. P. 1993 Excitation and evolution of unstable disturbances in supersonic boundary layer. *Proc. 1993 ASME Fluid Engineering Conference, Washington, DC, June 20–24*. FED-Vol. 151, pp. 1–13.

Fedorov, A. V. & Khokhlov, A. P. 2001 Prehistory of instability in a hypersonic boundary layer. *Theor. Comput. Fluid Dyn.* **14**, 359–375.

Fedorov, A. V. & Khokhlov, A. P. 2002 Receptivity of hypersonic boundary layer to wall disturbances. *Theor. Comput. Fluid Dyn.* **15**, 231–254.

Fedorov, A. V. & Tumin A. M. 2001 Initial-value problem for hypersonic boundary layer flows. *AIAA Paper* 2001-2781.

Gaponov, S. A. 1983 Excitation of unstable waves in supersonic boundary layer by sound. *Proc. 9th Canadian Congress of Applied Mechanics*, 30 May–3 June, Saskatoon, Canada (ed. H. T. Danyluk & P. B. Hertz), pp. 581–582.

Gaponov, S. A. 1985 On the development of disturbances in nonparallel supersonic flows. In *Laminar-Turbulent Transition* (ed. V. V. Kozlov), pp. 581–588. Springer.

Gaster, M. 1974 On the effects of boundary-layer growth on the flow stability. *J. Fluid Mech.* **66**, 465–480.

Goldstein, M. E. 1983 The evolution of Tollmien–Schlichting waves near a leading edge. *J. Fluid Mech.* **127**, 59–81.

Goldstein, M. E. 1985 Scattering of acoustic waves into Tollmein–Schichting waves by small streamwise variation in surface geometry. *J. Fluid Mech.* **154**, 509–529.

Graziosi, P. & Brown, G. L. 2002 Experiments on stability and transition at Mach 3. *J. Fluid Mech.* **472**, 83–124.

Kendall, J. M. 1975 Wind tunnel experiments relating to supersonic and hypersonic boundary layer transition. *AIAA J.* **13**, 290–299.

Kozlov, V. V. & Ryzhov, O. S. 1990 Receptivity of boundary layers: asymptotic theory and experiments. *Proc. R. Soc. Lond.* A **440**, 341–373.

Ma, Y. & Zhong, X. 2001 Numerical simulation of receptivity and stability of nonequilibrium reacting hypersonic boundary layers. *AIAA Paper* 2001-0892.

Mack, L. M. 1969 Boundary-layer stability theory. Part B. Doc. 900-277, JPL, Pasadena, California, May.

Mack, L. M. 1975 Linear stability theory and the problem of supersonic boundary-layer transition. *AIAA J.* **13**, 278–289.

Mack, L. M. 1987 Review of linear compressible stability theory. In *Stability of Time Dependent and Spatially Varying Flows* (ed. D. L. Dwoyer & M. Y. Hussaini). Springer.

Malik, M., Zang, T. & Bushnell, D. 1990 Boundary layer transition in hypersonic flows. *AIAA Paper* 90-5232.

Maslov, A. A., Shiplyuk, A. A., Sidorenko, A. A. & Arnal, D. 2001 Leading-edge receptivity of a hypersonic boundary layer on a flat plate. *J. Fluid Mech.* **426**, 73–94 (see also Preprint 1-97, Institute of Theoretical and Applied Mechanics SO RAN, Novosibirsk, 1997).

Morkovin, M. V. 1969 Critical evaluation of transition from laminar to turbulent shear layers with emphasis on hypersonically traveling bodies. *US Air Force Flight Dynamics Laboratory, Wright Patterson Air Force Base, Ohio*, AFFDL-TR, pp. 68–149.

Nayfeh, A. H. 1980 Stability of three-dimensional boundary layer. *AIAA J.* **18**, 406–416.

Reshotko, E. 1976 Boundary layer stability and control. *Annu. Rev. Fluid Mech.* **8**, 311–349.

Ruban, A. I. 1984 On Tollmien-Schilchting waves generation by sound. *Izv. Akad. Nauk SSSR. Mekh. Zhid. Gaza*, No. 6, 60–67.

Smith, F. T. 1989 On the first-mode instability in subsonic, supersonic or hypersonic boundary layers. *J. Fluid Mech.* **198**, 127–153.

Stetson, K. F., Kimmel, R. L., Thompson, E. R., Donaldson, J. C. & Siler, L. G. 1991 A comparison of planar and conical boundary layer stability and transition at a Mach number of 8. *AIAA Paper* 91-1639.

Tumin, A. M. & Fedorov, A. V. 1983 Spatial growth of disturbances in a compressible boundary layer. *J. Appl. Mech. Tech. Phys.* **24**, 548–554.

Wu, X. 1999 Generation of Tollmien–Schlichting waves by convecting gusts interacting with sound. *J. Fluid Mech.* **397**, 285–316.

Zhigulev, V. N. & Fedorov, A. V. 1987 On boundary layer receptivity to acoustic disturbances. *J. Prikl. Mekh. Tekh. Fiz.* No. 6, 43–49.

Zhigulev, V. N., Sidorenko, N. V. & Tumin, A. M. 1980 Generation of instability waves in a boundary layer by external turbulence. *J. Appl. Mech. Tech. Phys.* **21**, 774–780.

Zhigulev, V. N. & Tumin, A. M. 1987 *Onset of Turbulence*. Nauka, Novosibirsk.